

Electronic Supporting Information

In-Situ Solvothermal Reduction Engineering Enables Delicate Control Over Surface-rich Oxygen Vacancy on Bi₂WO₆ for Highly Efficient Photocatalytic CO₂ Reduction

Huanhuan Liu,^{‡a} Yanxu Chen,^{‡a} Wentao Wang,^{‡b} Xiaoyue He,^a Zixu He,^a Lei Li,^c Suyuan Zeng,^d

Ruiguo Cao,^a and Genqiang Zhang^{a*}

a Hefei National Research Center for Physical Sciences at the Microscale, CAS Key Laboratory of Materials for Energy Conversion, Department of Materials Science and Engineering, University of Science and Technology of China, Hefei, Anhui 230026 China.

b Guizhou Provincial Key Laboratory of Computational Nano-Material Science, Guizhou Education University, Guiyang, Guizhou 550018, China.

c School of Chemistry and Chemical Engineering, Hefei University of Technology, Hefei, Anhui, 230009, China.

d Department of Chemistry and Chemical Engineering, Liaocheng University, Liaocheng, Shandong, 252059, China.

[‡] These authors contribute equally.

* Corresponding Author

E-mail address: gqzhangmse@ustc.edu.cn (G.Q. Zhang)

1. Experimental

1.1 Synthesis of photocatalysts.

The Sur–Vo–BWO was prepared via a facile in-situ solvothermal reduction strategy. Typically, 1 mmol $\text{Na}_2\text{WO}_4 \cdot 2\text{H}_2\text{O}$ (Aladdin Industrial Corp., China) and 2 mmol $\text{Bi}(\text{NO}_3)_3 \cdot 5\text{H}_2\text{O}$ (Aladdin Industrial Corp., China) were added into 70 mL ethylene glycol (Sinopharm Chemical Reagent Corp., China) under vigorous magnetic stirring to obtain a homogeneous solution. The solution was then poured into a 100 mL Teflon-lined stainless autoclave and reacted at 120 °C for 18 h. Subsequently, the reaction temperature was raised to 180 °C for 6 h. After cooling the autoclave to room temperature in air, the product was centrifuged and washed consecutively with deionized water and ethanol, separately. The final product was dried at 70 °C in vacuum oven. As a contrast, the synthesis of BWO–L, Sur–Vo–BWO–3, Vo–BWO–H–9 and Vo–BWO–H were similar with Sur–Vo–BWO except maintained the reaction temperature at 120 °C for 24, 21, 15 and 9 h, and then raised to 180 °C for 0, 3, 9 and 12 h, respectively. The BWO–C was synthesized by calcining Sur–Vo–BWO at 450 °C in the air for 5 h.

1.2 Materials characterization:

The morphology of the as-prepared samples was observed by scanning electron microscopy (SEM, Hitachi SU8200, Japan) and transmission electron microscopy (TEM, Talox F200X, America). The X-ray diffraction (XRD, TTR-III, Japan) pattern with a Cu $\text{K}\alpha$ source was used to analyze crystalline structures. The chemical states of the as-prepared samples were performed with X-ray photoelectron spectroscopy (XPS, ESCA Lab MKII, UK) with Mg $\text{K}\alpha$ X-ray as the excitation source. Raman spectra were obtained by a confocal Raman microscope (LabRam HR, Japan) using a He/Ne laser

(532 nm) as the excitation source. The electron paramagnetic resonance (EPR) spectra were characterized by JES-FA200 (JEOL, Japan). The microwave frequency was 9.088 GHz. The microwave power was 0.998 mW. The modulation amplitude was 8.0 G. The modulation frequency was 100 kHz. And the experimental temperature was 25 °C. For the quantitative analysis of Vo, the 2, 2, 6, 6-tetramethylpiperidinyloxy (TEMPO) and Mn^{II} were employed as the standard sample and reference sample by using EPR methods, respectively.¹ 0.4991 g Vo-BWO-H photocatalysts were tested in the quantitative analysis. The optical character of the samples was obtained by UV-Vis diffuse reflectance spectra (UV-Vis DRS, SOLID3700, Japan). Photoluminescence (PL) spectra were measured on F-4600 PL spectrophotometer (Hitachi Ltd., Japan) at room temperature. The excited wavelength and excited slit are 345 nm and 5.0 nm, separately. The emission spectra are around 400-800 nm. Time-resolved PL spectra were acquired using a time-corrected single photon counting system (Fluorohub, Horiba Scientific, Japan) with an excitation wavelength of 370 nm at room temperature. In-situ Fourier transform infrared spectroscopy (FTIR) spectra were acquired using a Thermo Scientific Nicolet iS50 FTIR Spectrometer. The FTIR curve at 0 min was used as the baseline.

1.3 Electrochemical measurements

Electrochemical measurements were carried out by a CH Instruments 660E electrochemical workstation in a three-electrode cell using platinum wire, fluorine doped tin oxide (FTO) coated with catalysts and Ag/AgCl as the counter electrode, working electrode and reference electrode, respectively. 0.5 M Na₂SO₄ was saturated by Ar in the room temperate (25 °C) as the electrolyte at the 0 V bias potential vs. Ag/AgCl electrode. A simulated sunlight irradiation (300 W xenon lamp,

AM 1.5 G, 100 mW cm⁻²) was applied as a light source in transient photocurrent responses curves and electrochemical impedance spectrum plots.

The details of the working electrodes were described as follows: 5 mg catalysts were dispersed in 1 mL absolute ethanol and 5 uL nafion by sonication. Then, 10 μL of the suspension was drop-coated at FTO glass with an area of 1 × 1 cm². The FTO glasses were dried at 80 °C for 24 h in vacuum oven to remove volatile organic compound before using.

1.4 Photocatalytic CO₂ reduction tests

The photocatalytic CO₂ reduction testing was implemented by a Labsolar-6A (Beijing PerfectLight Co. Ltd, China) all glass automatic on-line trace gas analysis system with a 500 mL Pyrex reactor as reaction chamber. The reaction chamber was connected to a water bath for maintaining the reaction temperature at 5 °C. Typically, 25 mg samples were dispersed on a quartz disc (65 mm for diameter). The quartz disc was enclosed in the reaction chamber and then vacuumed to remove air in the on-line analysis system. 5 mL of deionized water and a certain volume of high-purity CO₂ (99.99%) were injected into the reaction systems to ensure constant pressure of 80 kPa before photocatalytic test. A 300 W Xe lamp (PLSSXE 300, Beijing PerfectLight Co., Ltd. China) was employed as the light source in the photocatalytic test. The average value of light intensity (\bar{I}) is 20.4 mW cm⁻² detected by photometer (ST-85, Beijing Normal University Photoelectric Technology Co. LTD, China) and calculated by eqn (1). The evolution of CO and CH₄ were determined by a gas chromatograph (GC 7900, Techcomp, China, Ar carrier).

$$\bar{I} = \frac{2}{3}\bar{I}_{edge} + \frac{1}{3}\bar{I}_{center}$$

(1)

Where \bar{I}_{edge} and \bar{I}_{center} are the average value of light intensity at edge and centre region, as shown in Fig. S10.

The total electron transfer rate (R_{TET}) was used to characterize the separation capacity of photoinduced electron-hole pairs, which was calculated by using the following eqn (2):

$$R_{TET} = 2 \times R_{CO} + 4 \times R_{CH_4} \quad (2)$$

where R_{CO} and R_{CH_4} are the CO and CH_4 evolution rate, disparately.

The apparent quantum yield (AQY) for CO was calculated using the following eqn (3):

$$AQY = \frac{2 \times \text{Number of evolved CO molecules}}{\text{Numer of incident photons}} \times 100\% = \frac{2 \times N \times N_A \times h \times c}{\bar{I} \times S \times \lambda \times t} \times 100\% \quad (3)$$

Where \bar{I} is 5.1, 14.3 and 14.1 mW cm^{-2} at 420, 500 and 600 nm, respectively. N is CO evolution amount (mol). t is the irradiation time (s). λ is the irradiation wavelength number (m). N_A is the Avogadro constant ($6.022 \times 10^{23} \text{ mol}^{-1}$). S is the irradiation area (cm^2). h is the Planck constant ($6.63 \times 10^{-34} \text{ J}\cdot\text{s}$). And c is the light speed ($3 \times 10^8 \text{ m s}^{-1}$).

1.5 Density functional theory (DFT) calculation details

DFT based first-principles calculations were performed using the projected augmented wave method implemented in the Vienna *ab initio* simulation package

(VASP).^{2, 3} The Kohn–Sham one-electron states were expanded using the plane-wave basis set with a kinetic energy cutoff of 500 eV. The Perdew–Burke–Ernzerh of exchange-correlation functional within the generalized gradient approximation was employed for the geometrical optimization.⁴ The Brillouin-zone integration was carried out using the Monkhorst-Pack sampling method with a density of $3 \times 3 \times 1$.⁵ A vacuum layer of 15 Å was included to avoid the interaction between neighboring slabs. All atoms were fully relaxed until the maximum magnitude of the force acting on the atoms was smaller than 0.03 eV/Å. Following the reference, the BWO (001) surface was modelled by a periodic seven-layer slab repeated in a 2×2 surface unit cell to study surface reactions' mechanistic chemistry.⁶ For O vacancy calculations, one atom was removed from this 2×2 supercell, and the remaining atoms were allowed to relax. The photocatalytic CO₂ reduction properties of BWO and Vo–BWO under acidic conditions (pH = 0) have been investigated through the Concerted Proton–Electron Transfer mechanism.⁷ First, BWO and Vo–BWO (denoted as *) absorb a CO₂ molecule from the solution and subsequently release H⁺ + e⁻ pairs, leading to the formation of *COOH. Then, another H⁺ + e⁻ pairs were added and reacts with *COOH to form *CO, while releasing a molecule of H₂O. Finally, *CO was desorbed from the substrate. The whole basic steps of photocatalytic CO₂ reduction could be described as following eqn (4)-(7):



In the actual reaction, although the electrons come from the photogenerated electrons in the excited state of the material and the H⁺ originates from the cleavage of water molecules in solution, we still equated the free energy of the H⁺+ e⁻ pairs to half the free energy of an isolated H₂ molecule after using a computational hydrogen electrode.⁸ Thus, the Gibbs free energy of the reaction can be obtained by the following eqn (8)-(11):

$$\Delta G_1 = G(\text{CO}_2) - G(*) - G(\text{CO}_2) \quad (8)$$

$$\Delta G_2 = G(*\text{COOH}) - G(*\text{CO}_2) - 0.5 \times G(\text{H}_2) \quad (9)$$

$$\Delta G_3 = G(*\text{CO}) + G(\text{H}_2\text{O}) - G(*\text{COOH}) - 0.5 \times G(\text{H}_2) \quad (10)$$

$$\Delta G_4 = G(*) + G(\text{CO}^*) - G(*\text{CO}) \quad (11)$$

The Gibbs free energy is defined as: $G = \Delta E + (\Delta\text{ZPE} - T\Delta S)$, where ΔE is the total energy based on DFT calculations, ΔZPE is the zero point energy (ZPE) correction, T is the temperature (here T is 298.15K), and ΔS is the entropy change.

For the calculation of excited states, the FERWE and FERDO parameters could be modulated in the VASP program. This allows one of the electrons to leap from the valence band maximum (VBM) so that a photogenerated electron is produced in the conduction band minimum (CBM) and a photogenerated hole is produced in the VBM.⁹ Since in practice the photoexcitation is localized, we need to use sufficiently large supercells to obtain more reasonable results. Here we used a 4 × 4 supercell. The different supercell was used in the part of theory calculation in order to better match the actual situation. In photocatalytic CO₂ reduction process, abundant CO₂ molecules are adsorbed in catalyst surface, which indicate that it is not reasonable to adsorb only one CO₂ molecule in a 4*4 supercell. Therefore, the 2*2 supercells instead of 4*4 supercells were used in the free energy step diagram in order to meet

practical conditions. As for the excited state calculation model, 4*4 supercells instead of 2*2 supercells were used, that is because only a tiny fraction of the electrons in the actual material are excited. Obviously, the larger the number of supercells we choose, the closer the simulation will be to reality. For the excited state calculation of Vo-BWO, one atom was still removed from this 4 × 4 supercell and the rest of the atoms could relax.

2. Figures

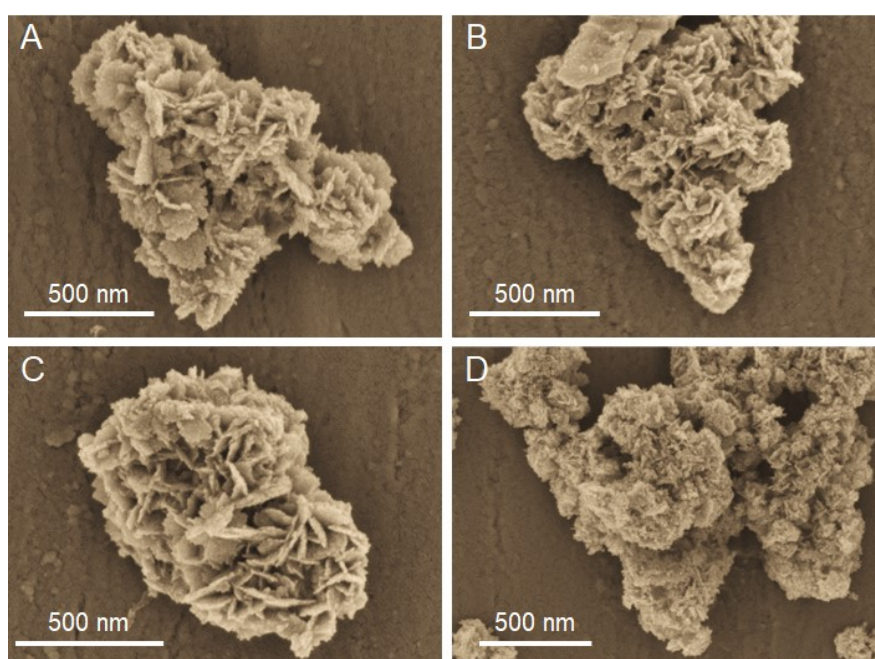


Fig. S1 SEM images of the as-prepared (a) BWO-L, (b) Sur-Vo-BWO, (c) Vo-BWO-H and (d) BWO-C.

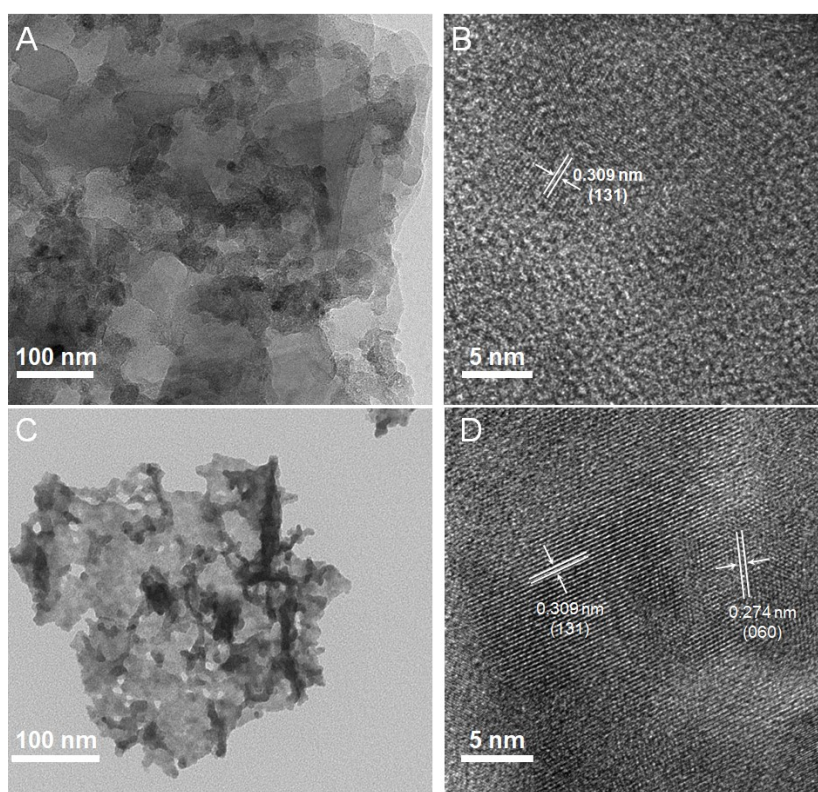


Fig. S2 (A) TEM image and (B) HRTEM image of BWO-L, respectively; (C) TEM image and (D) HRTEM image of BWO-C, respectively.

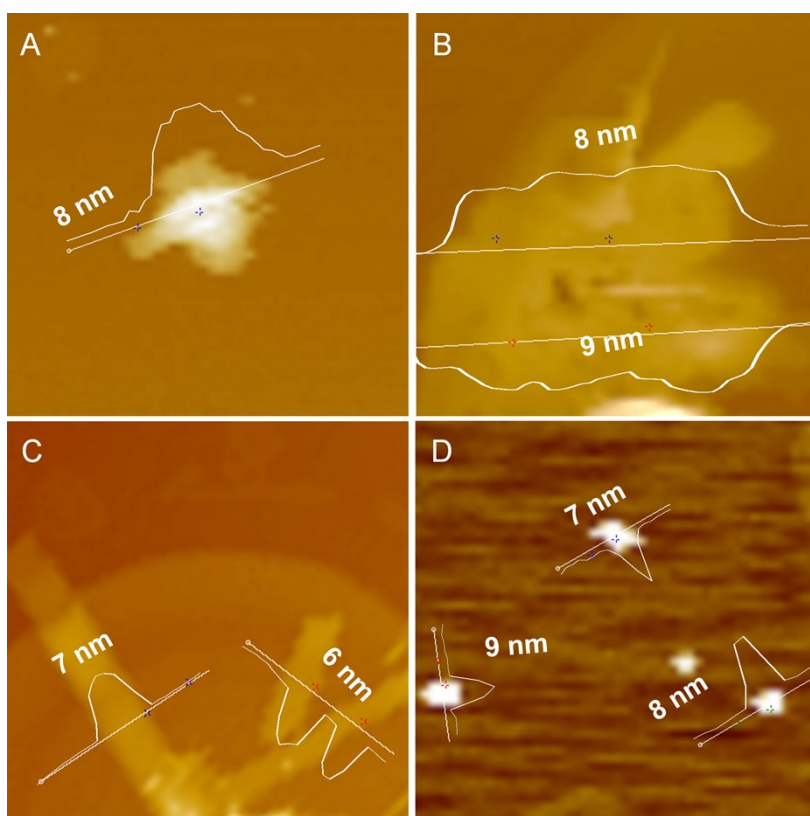


Fig. S3 AFM image and the corresponding height profiles of (A) BWO-L, (B) Sur-Vo-BWO, (C) Vo-BWO-H and (D) BWO-C.

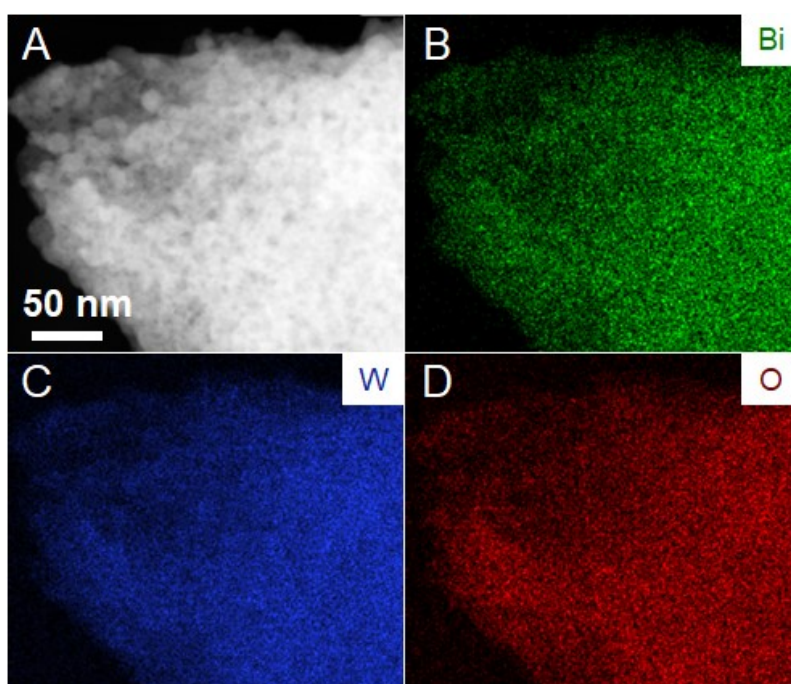


Fig. S4 Elemental mapping images of Sur-Vo-BWO.

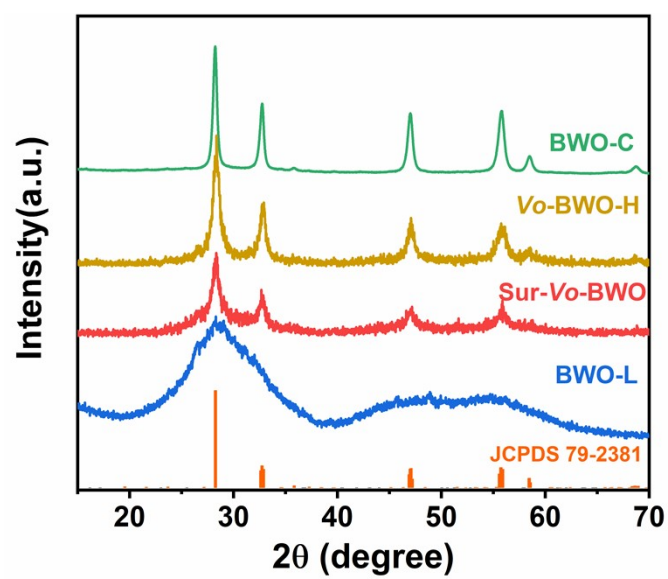


Fig. S5 XRD pattern of as-obtained samples.

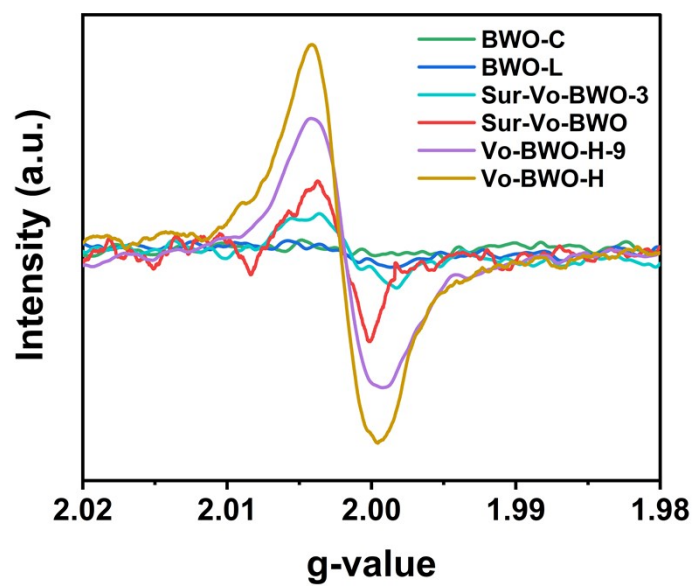


Fig. S6 (A) EPR spectra of as-obtained samples.

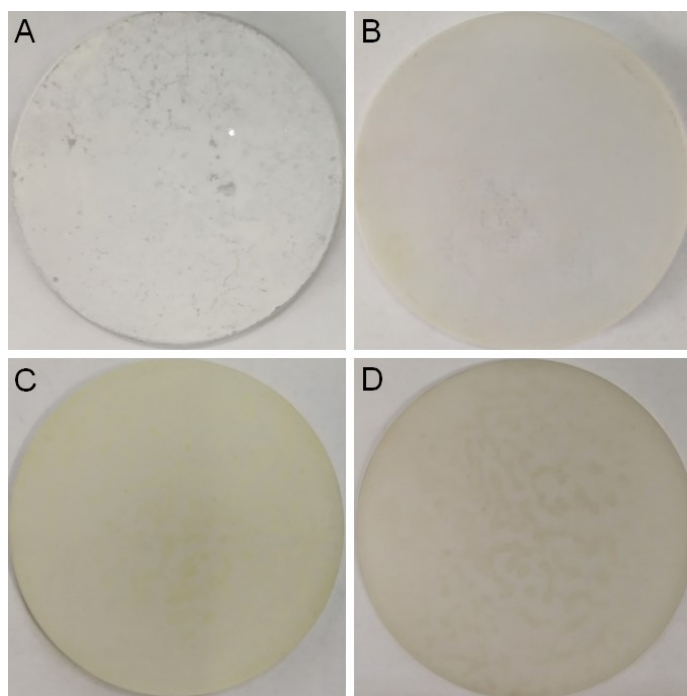


Fig. S7 The photograph of (A) BWO-C, (B) BWO-L, (C) Sur-Vo-BWO and (D) Vo-BWO-H dispersed on a quartz disc with diameter of 65 cm.

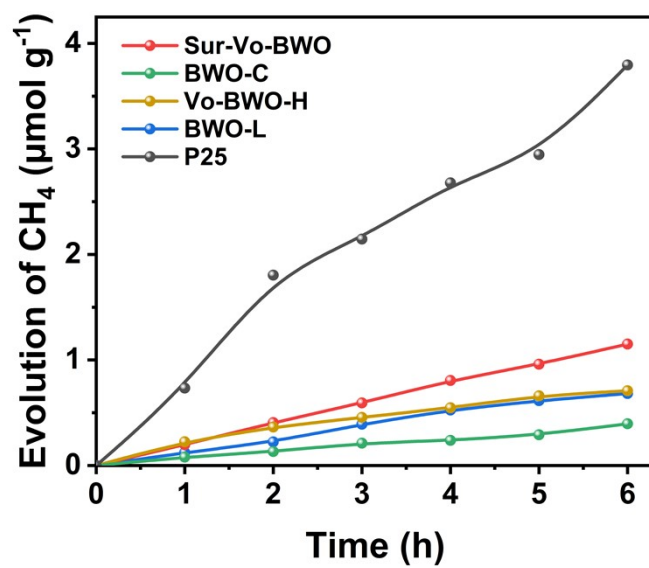


Fig. S8 Time courses of photocatalytic CH₄ evolution curves of as-obtained BWO samples and P25.

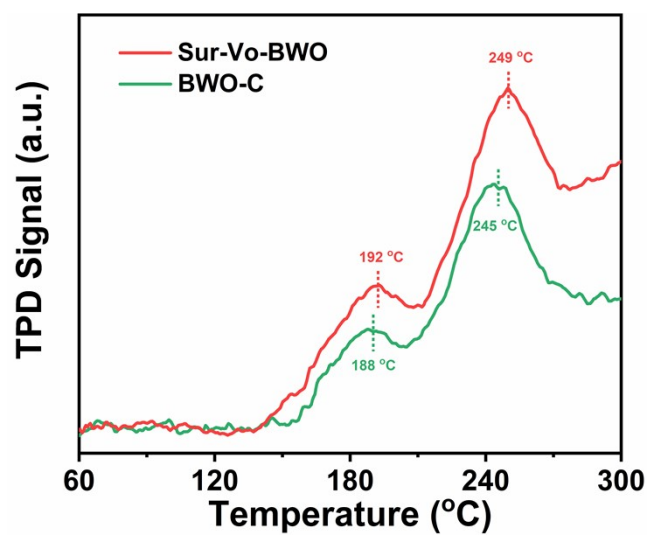


Fig. S9 CO temperature-programmed desorption spectra of Sur-Vo-BWO and BWO-C.

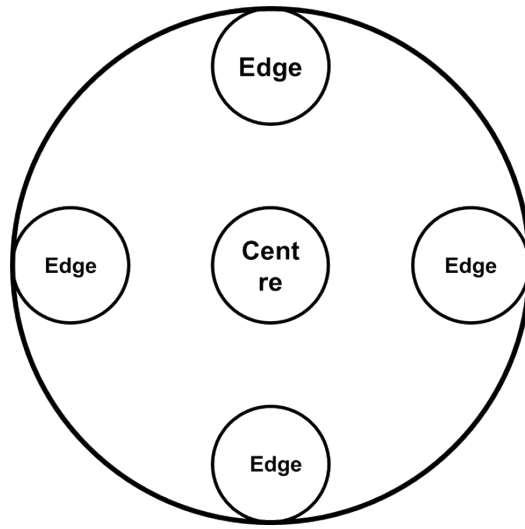


Fig. S10 The measured sites of light intensity.

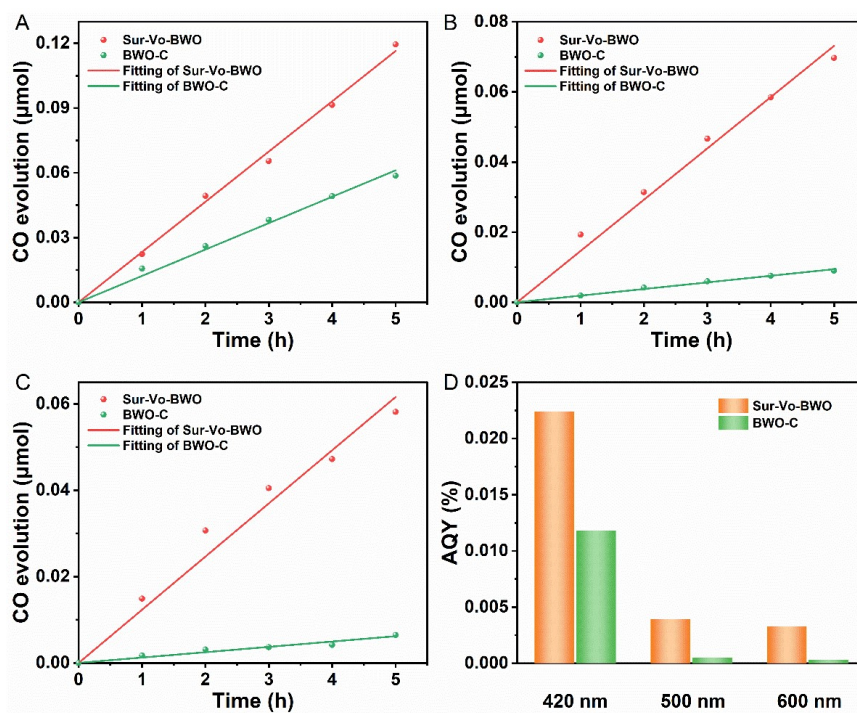


Fig. S11 Time course of CO evolution over Sur-Vo-BWO and BWO-C under (A) 420 nm (B) 500 nm and (C) 600 nm monochromatic light irradiation; (D) AQY of CO evolution over Sur-Vo-BWO and BWO-C under different monochromatic light irradiation.

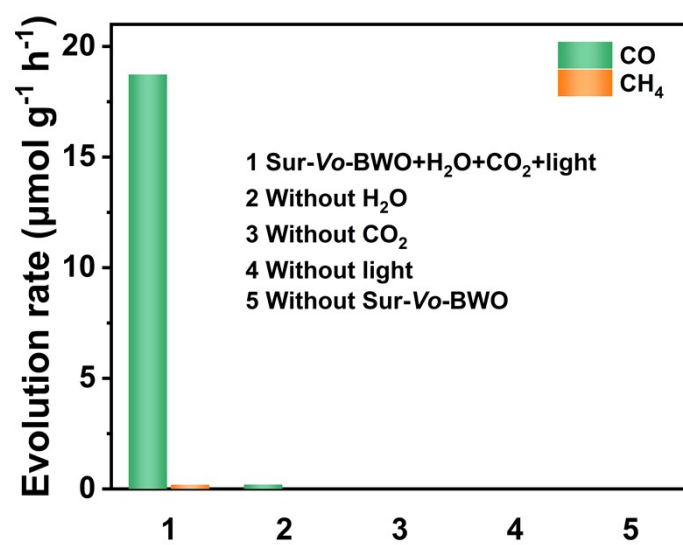


Fig. S12 CO₂ reduction activities of Sur-Vo-BWO under various conditions.

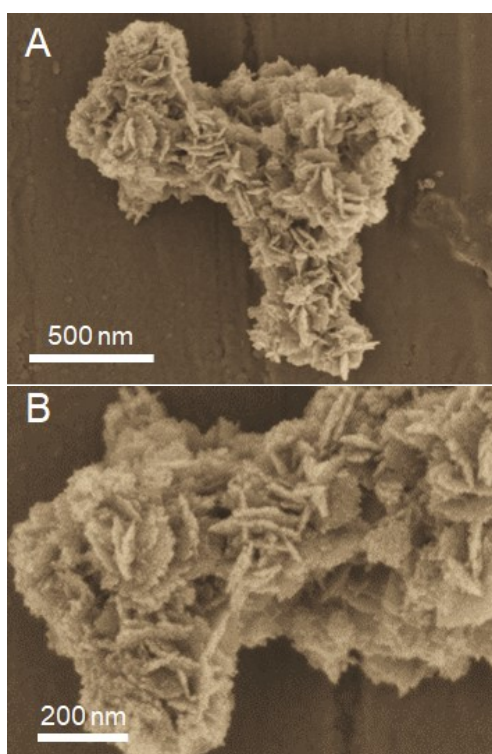


Fig. S13 SEM images of Sur-Vo-BWO after photocatalytic cycle test.

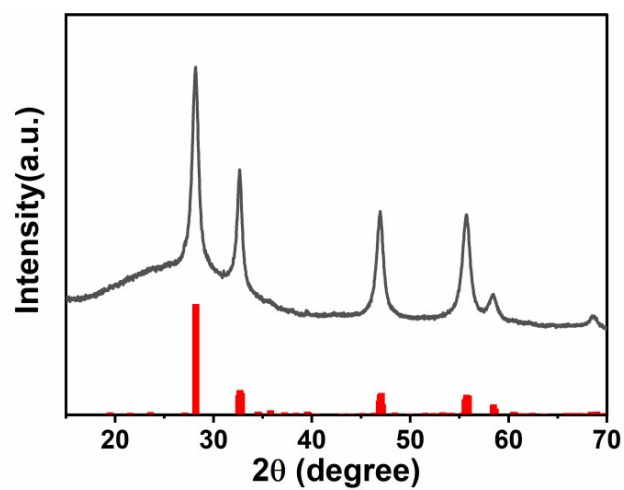


Fig. S14 XRD patterns of the Sur-Vo-BWO after photocatalytic cycle test.

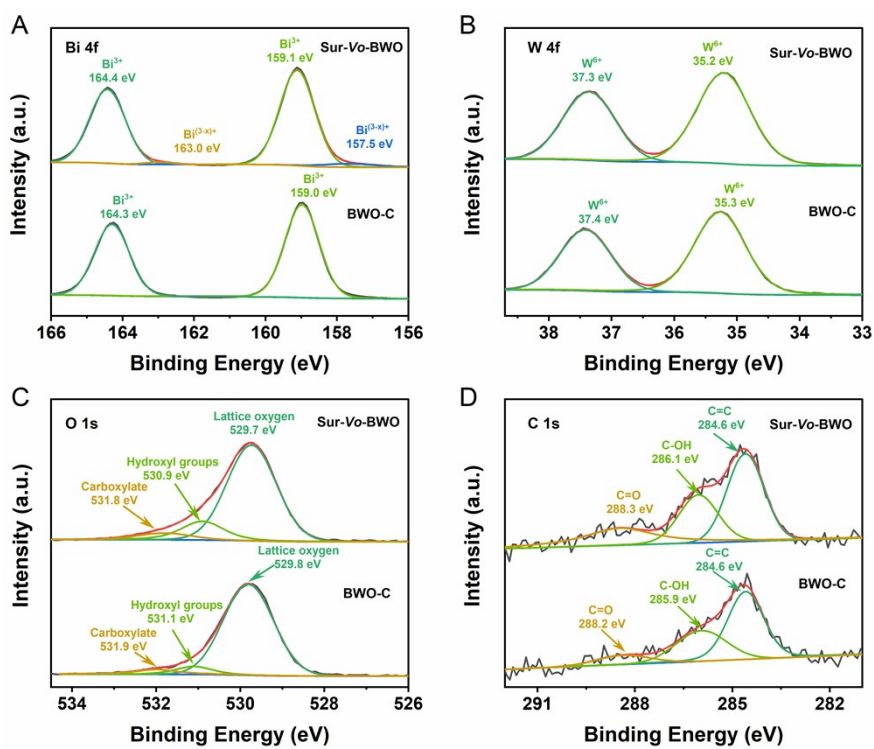


Fig. S15 High resolution XPS spectra for Sur-Vo-BWO and BWO-C after cycle testing:

(A) Bi 4f, (B) W 4f, (C) O 1s and (D) C 1s, respectively.

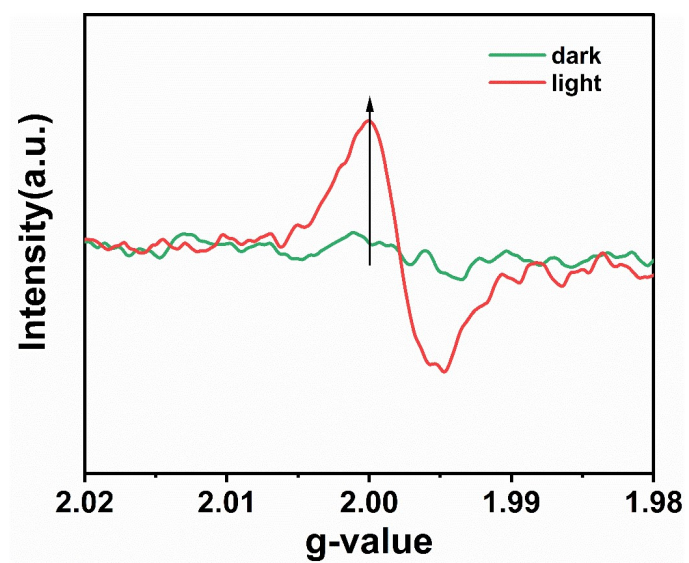


Fig. S16 EPR spectra of Sur-Vo-BWO after photocatalytic cycle test in the dark and under light illumination.

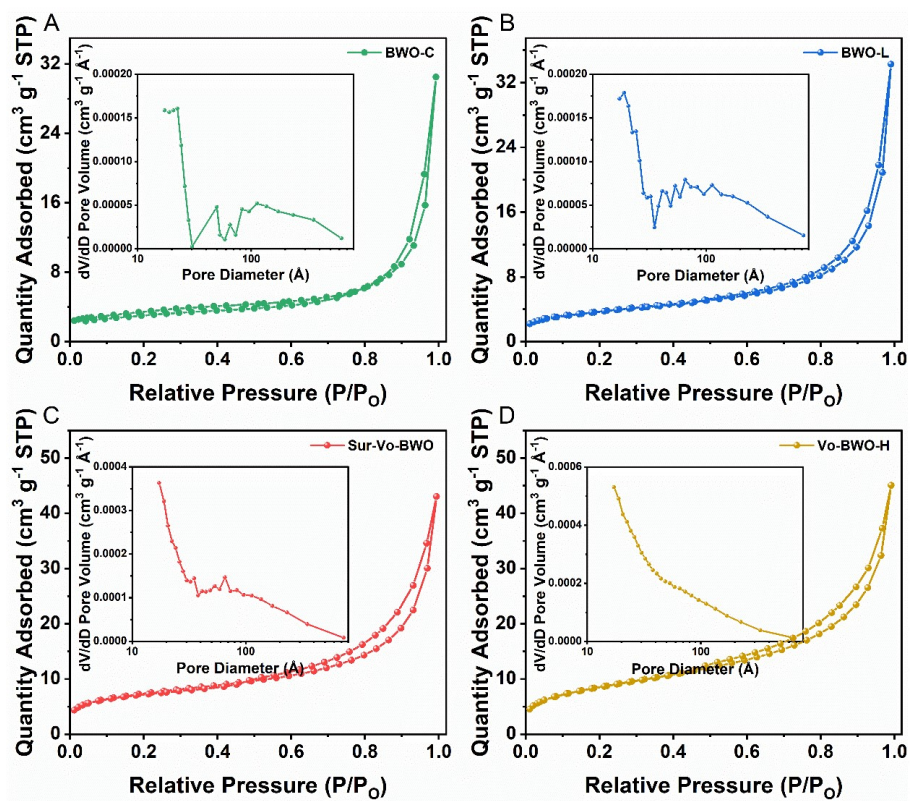


Fig. S17 N_2 adsorption-desorption isotherm and corresponding pore size distribution curve of (A) BWO-C, (B) BWO-L, (C) Sur-Vo-BWO and (D) Vo-BWO-H.

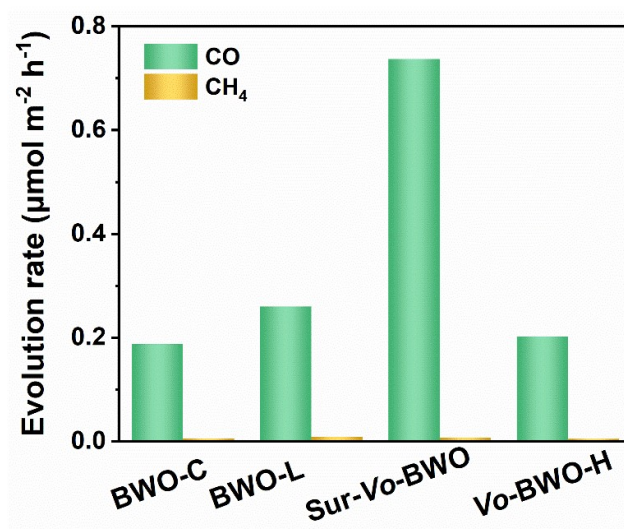


Fig. S18 The specific area normalized CO₂ photoreduction rate for Sur-Vo-BWO and control samples.

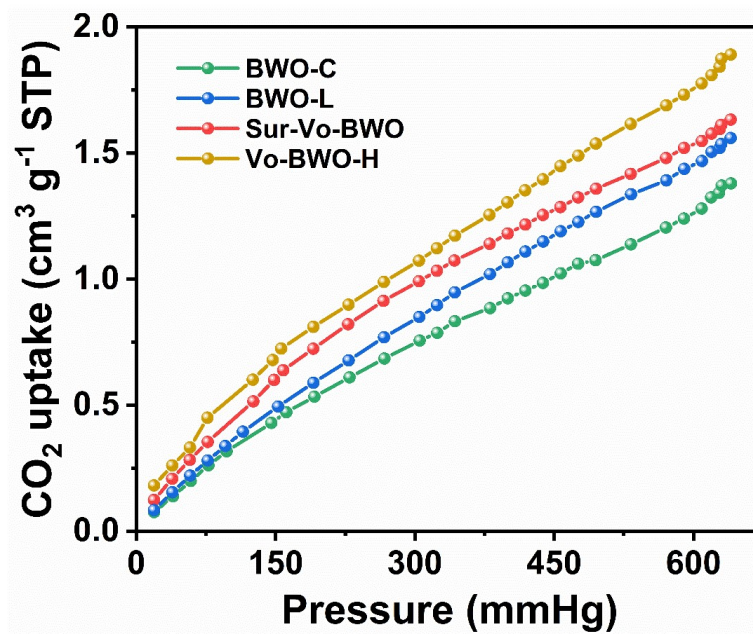


Fig. S19 CO₂ adsorption isotherms of as-obtained samples.

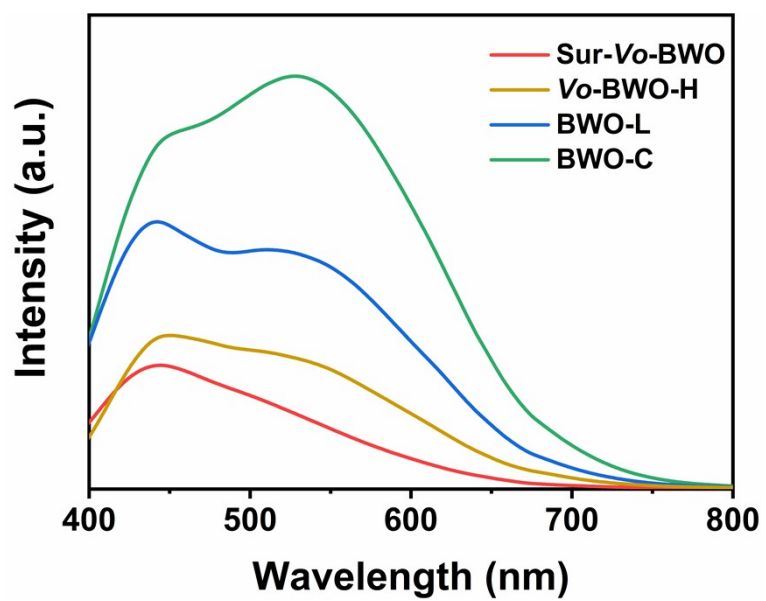


Fig. S20 Steady-state PL spectra of as-obtained samples.

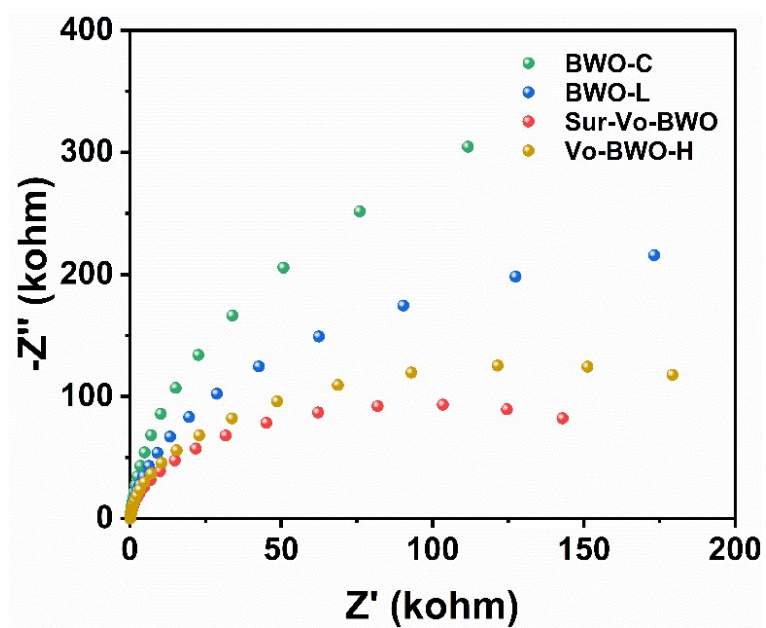


Fig. S21 EIS plots of the as-prepared samples under a simulated sunlight irradiation.

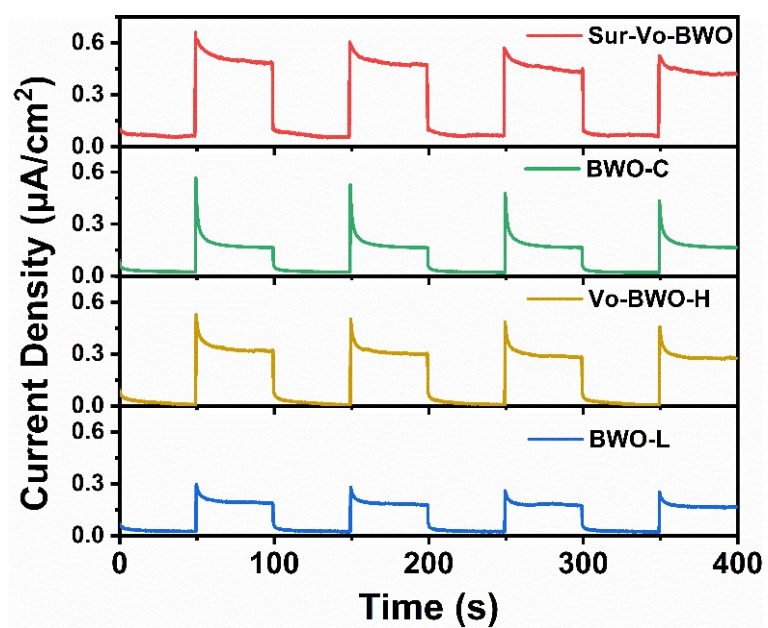


Fig. S22 Transient photocurrent responses curves of the as-prepared samples.

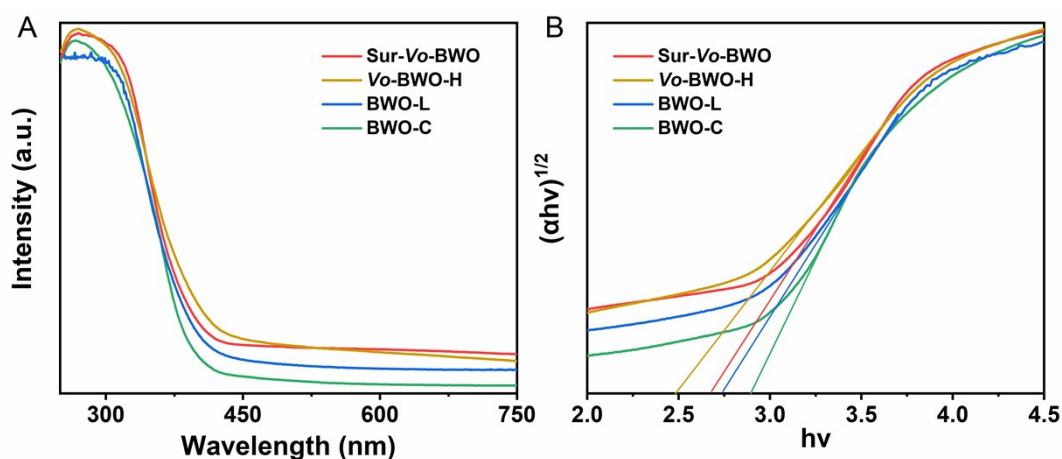


Fig. S23 (A) UV-Vis DRS and (B) corresponding Kubelka-Munk plots for the band gap estimation of as-obtained samples.

The optical property is evaluated by UV-Vis DRS spectra. The BWO-C expose inferior optical respond in visible light region. However, the light absorption extends to the longer wavelengths with extension the solvothermal time at high temperature, which is due to the Vo on the surface of BWO. The band gap is calculated as 2.89, 2.75, 2.67 and 2.49 eV for BWO-C, BWO-L, Sur-Vo-BWO and Vo-BWO-H, respectively. The narrower band gap and extended absorption in the visible-light region improve the utilization for low energy light, which is the major component of sun light on the earth.^{10, 11} The above-mentioned results indicate that Vo offers additional light harvesting in the visible-light region, while BWO-C mainly in UV region.

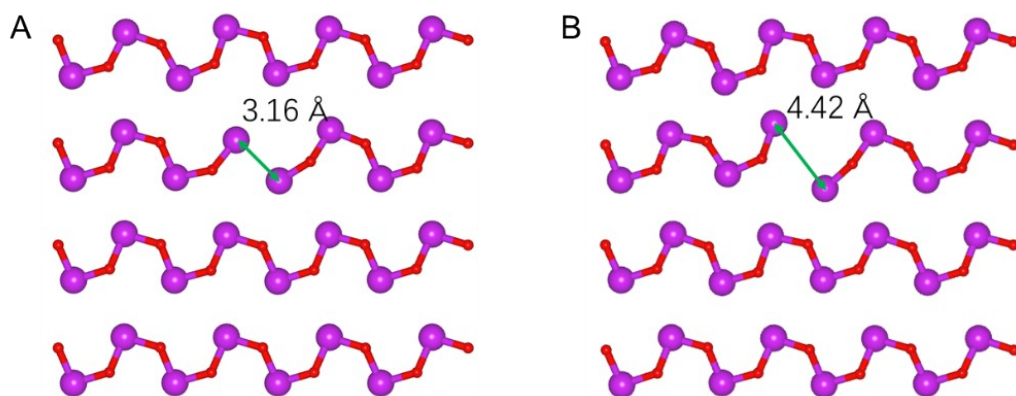


Fig. S24 The distance of Bi–vacancy–Bi (A) on ground state and (B) under excited state.

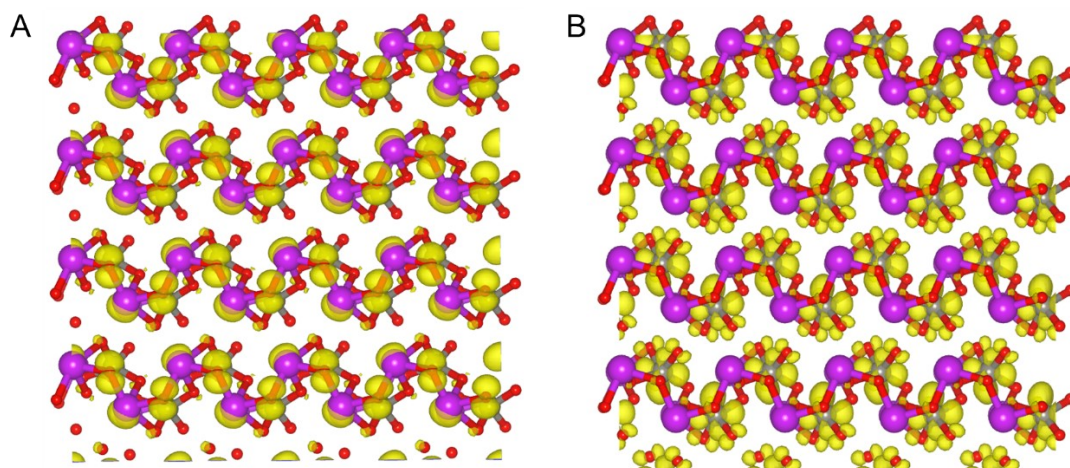


Fig. S25 Charge difference of (A) photoinduced electron and (B) photoinduced hole for BWO under excited state.

Tables

Table S1. Relative ratio of lattice oxygen and Vo determined by O 1s XPS

Samples	Lattice oxygen	Vo
BWO-C	84.98%	15.02%
Sur-Vo-BWO	77.34%	22.66%
Sur-Vo-BWO after 30s Ar ⁺ etching	81.48%	18.52%
Sur-Vo-BWO after 60s Ar ⁺ etching	83.74%	16.26%

Table S2. Transfer numbers of photo-induced electrons based on the evolution rate of CO and CH₄.

Sample	CO evolution rate ($\mu\text{mol g}^{-1} \text{h}^{-1}$)	CH ₄ evolution rate ($\mu\text{mol g}^{-1} \text{h}^{-1}$)	Total electron transfer rate ($\mu\text{mol}_e \text{g}^{-1} \text{h}^{-1}$)	Selectivity of CO (%)
BWO-C	2.249	0.066	5.026	97.1
BWO-L	3.450	0.114	7.812	96.8
Sur-Vo-BWO	18.727	0.192	38.990	99.0
Vo-BWO-H	6.180	0.155	13.600	97.6
P25	1.742	0.638	8.588	73.2

Table S3. Summary of the photocatalytic CO evolution performance of some Bi₂WO₆-based catalysts.

Photocatalyst	Reaction medium	Light source	CO evolution rate (μmol g ⁻¹ h ⁻¹)	Ref.
Sur-Vo-BWO	H ₂ O vapor	300 W Xe lamp	18.73	This work
Bi₂WO₆			0.77	
Bi₂WO₆-V₁	H ₂ O vapor	300 W Xe lamp	3.8	12
Bi₂WO₆-V₂			7.7	
Bi₂WO₆	H ₂ O vapor	300 W Xe lamp	0.81	13
g-C₃N₄/Bi₂WO₆		λ > 420 nm	5.19	
Bi₂WO₆	H ₂ O vapor	300 W Xe lamp	4.14	14
Bi₂WO₆/Bi₂O₃		λ > 420 nm	17.39	
BWO/ C₃N₄			6.38	
RGO/ C₃N₄	H ₂ O vapor	300 W Xe lamp	4.20	15
Bi₂WO₆/RGO/C₃N₄		λ > 420 nm	15.96	
Bi₂WO₆	MeCN/ H ₂ O/	300 W Xe lamp	16.8	16
Vo-Bi₂WO₆	TEOA		40.6	
Bi₂O₂CO₃/Bi/Bi₂WO₆	H ₂ O	300 W Xe lamp	0.818	17
Bi₂WO₆/TiO₂	H ₂ O vapor	300 W Xe lamp	2.6	18
PB-Bi₂WO₆		300 W Xe lamp	0.333	19
PB₅₅₀-Bi₂WO₆	H ₂ O vapor	600>λ>420 nm	0.50	
Cs₃Bi₂I₉/Bi₂WO₆	H ₂ O vapor	300 W Xe lamp	7.33	20

Bi₂WO₆-nanosheets			1.80	
	H ₂ O vapor	300 W Xe lamp		21
Bi₂WO₆-C2			7.12	
Vo-Bi₂WO₆/Au			34.8	
	H ₂ O vapor	300 W Xe lamp		22
Vo-Bi₂WO₆			3.7	
		300 W Xe lamp	17.97	
Bi₂WO₆/InVO₄	H ₂ O vapor			23
		$\lambda > 420$ nm	0.8	

Table S4. Relative ratio of lattice oxygen, surface hydroxyl groups and carboxylate determined by O 1s XPS after cycle test.

Samples	Lattice oxygen	Hydroxyl groups	Carboxylate
Sur-Vo-BWO	78.04%	15.50%	6.36%
BWO-C	87.25%	6.87%	5.88%

Table S5. Relative ratio of C=C, C-OH and C=O determined by C 1s XPS after cycle test.

Samples	C=C	C-OH	C=O
Sur-Vo-BWO	46.67%	28.40%	24.93%
BWO-C	61.24%	23.61%	15.15%

Table S6. The specific area normalized CO₂ photoreduction rate and total electron transfer rate of Sur-Vo-BWO and control samples.

Sample	CO evolution rate ($\mu\text{mol m}^{-2} \text{h}^{-1}$)	CH ₄ evolution rate ($\mu\text{mol m}^{-2} \text{h}^{-1}$)	Total electron transfer rate ($\mu\text{mol}_e \text{m}^{-2} \text{h}^{-1}$)	Selectivity of CO (%)
BWO-C	0.188	0.00553	0.399	97.1
BWO-L	0.260	0.00860	0.555	96.8
Sur-Vo-BWO	0.737	0.00755	1.110	99.0
Vo-BWO-H	0.202	0.00508	0.425	97.6

Table S7. Parameters of the time-resolved photoluminescence decay curves.

Sample	τ_1 (ns)	τ_2 (ns)	τ_{ave} (ns)
BWO-C	0.207 (77.7%)	6.319 (22.3%)	1.57
Sur-Vo-BWO	0.255 (71.6%)	8.813 (28.4%)	2.69

Reference:

1. C. Mao, H. Cheng, H. Tian, H. Li, W.-J. Xiao, H. Xu, J. Zhao and L. Zhang, *Appl. Catal. B: Environ.*, 2018, **228**, 87-96.
2. G. Kresse and J. Hafner, *Phys. Rev. B*, 1993, **47**, 558-561.
3. G. Kresse and J. Furthmüller, *Phys. Rev. B*, 1996, **54**, 11169.
4. J. P. Perdew, K. Burke and M. Ernzerhof, *Phys. Rev. Lett.*, 1996, **77**, 3865.
5. H. J. Monkhorst and J. D. Pack, *Phys. Rev. B*, 1976, **13**, 5188.
6. Y. Wu, J. Zhang, B. Long and H. Zhang, *Appl Surf Sci*, 2021, **548**, 149053.
7. M. T. Koper, *Chem. Sci.*, 2013, **4**, 2710-2723.
8. J. K. Nørskov, J. Rossmeisl, A. Logadottir, L. Lindqvist, J. R. Kitchin, T. Bligaard and H. Jonsson, *J. Phys. Chem. B*, 2004, **108**, 17886-17892.
9. J. Huang, Y. Peng, J. Jin, M. S. Molokeev, X. Yang and Z. Xia, *J. Phys. Chem. Lett.*, 2021, **12**, 12345-12351.
10. H. Liu, K. Tian, J. Ning, Y. Zhong, Z. Zhang and Y. Hu, *ACS Catal.*, 2019, **9**, 1211-1219.
11. H. Liu, L. Li, C. F. Guo, J. Q. Ning, Y. J. Zhong and Y. Hu, *Chem. Eng. J.*, 2020, **385**, 123929.
12. C. Lu, X. Li, Q. Wu, J. Li, L. Wen, Y. Dai, B. Huang, B. Li and Z. Lou, *ACS Nano*, 2021, **15**, 3529-3539.
13. M. Li, L. Zhang, X. Fan, Y. Zhou, M. Wu and J. Shi, *J. Mater. Chem. A*, 2015, **3**, 5189-5196.
14. Z. Xie, Y. Xu, D. Li, S. Meng, M. Chen and D. Jiang, *ACS Appl. Energy Mater.*, 2020, **3**, 12194-12203.
15. W.-K. Jo, S. Kumar, S. Eslava and S. Tonda, *Appl. Catal. B: Environ.*, 2018, **239**, 586-598.
16. Q. Li, X. Zhu, J. Yang, Q. Yu, X. Zhu, J. Chu, Y. Du, C. Wang, Y. Hua, H. Li and H. Xu, *Inorg. Chem. Front.*, 2020, **7**, 597-602.
17. Y. Zhang, L. Wang, F. Dong, Q. Chen, H. Jiang, M. Xu and J. Shi, *J. Colloid Interface Sci.*, 2019, **536**, 575-585.
18. L. Yuan, K.-Q. Lu, F. Zhang, X. Fu and Y.-J. Xu, *Appl. Catal. B: Environ.*, 2018, **237**, 424-431.
19. Z. Sun, Z. Yang, H. Liu, H. Wang and Z. Wu, *Appl Surf Sci*, 2014, **315**, 360-367.
20. Z.-L. Liu, R.-R. Liu, Y.-F. Mu, Y.-X. Feng, G.-X. Dong, M. Zhang and T.-B. Lu, *Solar RRL*, 2021, **5**, 2000691.
21. Y. Liu, D. Shen, Q. Zhang, Y. Lin and F. Peng, *Appl. Catal. B: Environ.*, 2021, **283**, 119630.
22. Y. Wang, T. Chen, F. Chen, R. Tang and H. Huang, *Sci. Chian Mater.*, 2022.
23. J. Li, F. Wei, Z. Xiu and X. Han, *Chem. Eng. J.*, 2022, **446**, 137129.